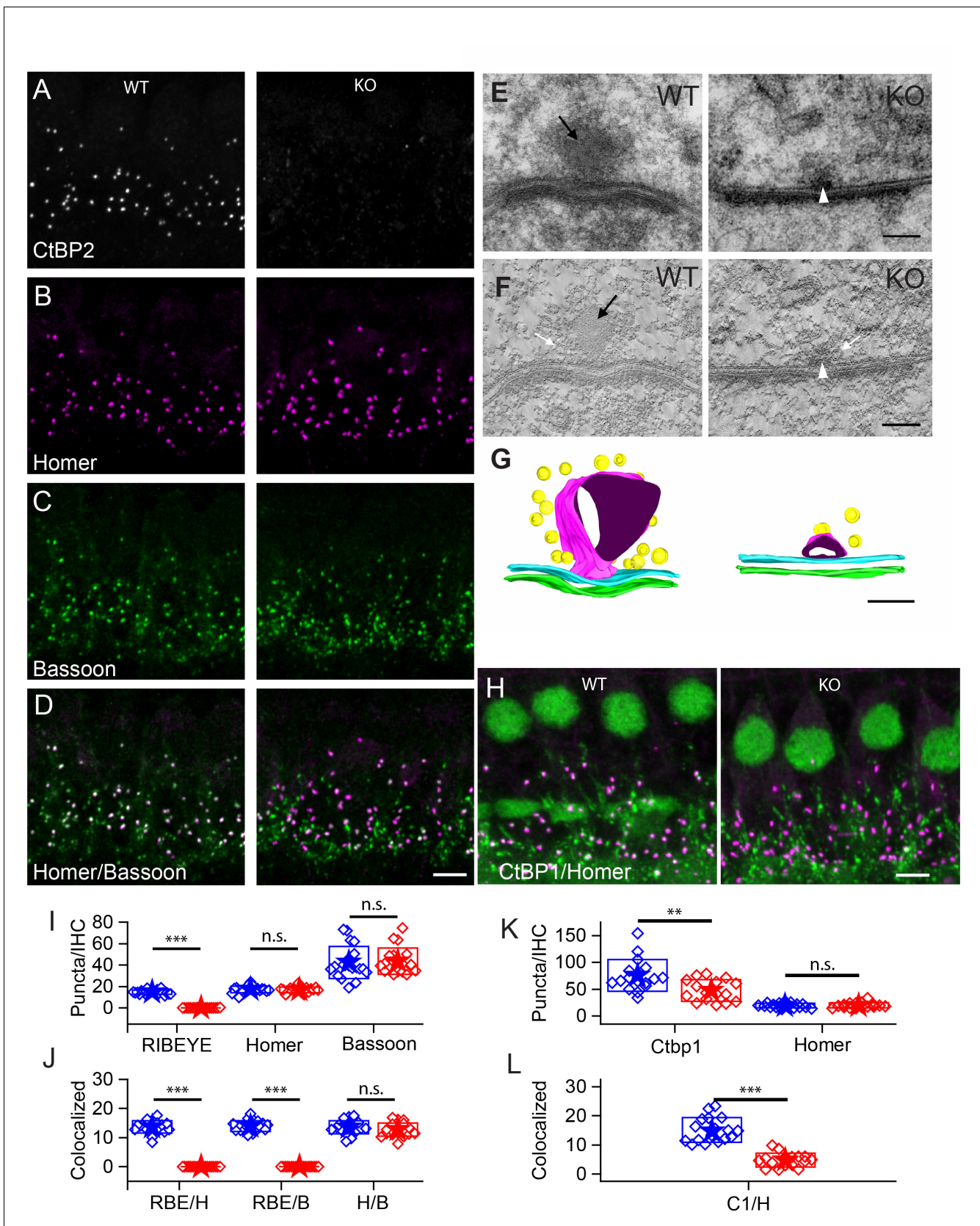# Figures and figure supplements

The presynaptic ribbon maintains vesicle populations at the hair cell afferent fiber synapse

Lars Becker *et al*

Figure 1. Number of synapses stays unaffected in ribbon-less organs of corti. (A–D) Maximum intensity projections of confocal z-sections of inner hair cells (IHCs) in apical cochlea turns of P22 KO and wildtype littermates, immunolabeled for CtBP2/RIBEYE (A), Homer (B), Bassoon (C) and Homer-

Figure 1 continued on next page

Figure 1 continued

Bassoon Overlay (D). Virtually no punctated extra-nuclear CtBP2 staining that is colocalized with other synaptic proteins can be seen in KO mice, whereas Bassoon and Homer appear generally unaffected. (E) 100 nm thick transmission electron microscopy (TEM) sections of pre- and postsynaptic densities in WT and KO mice at P28 confirm the absence of electron-dense ribbon structures in KO mice. (For E-–G) Black arrows point to ribbon structure, white arrows point to synaptic vesicles and white arrowheads point to the remaining density resembling the arciform density. (F) Single slice from a 10-nm thick tomographic section. (G) Reconstruction of complete synapses from data used to create E,F. Presynaptic density in cyan and postsynaptic density in green. Tethered synaptic vesicles modeled in yellow, electron-dense structure attributed to synaptic ribbons in magenta. (H) Confocal maximum intensity projection of IHCs immunolabeled for CtBP1 (green) and Homer (magenta). (I) Quantification of RIBEYE, Homer and Bassoon puncta in the organ of corti normalized to the number of IHCs in analyzed regions of interest, showing complete loss of synaptic RIBEYE staining in KO. The amount of Homer and Bassoon staining is unaffected ($p>0.05$). WT in blue, n = 20 mice, quantified puncta —RIBEYE = 3796, Bassoon = 10,215, Homer = 4340; KO in red, n = 19 mice, n puncta — RIBEYE = 33, Bassoon = 10,825, Homer = 4201. (J) Paired synaptic puncta per IHC is lost in the absence of RIBEYE staining ($p \leq 0.001$) between WT and KO. The number of synapses defined by colocated postsynaptic Homer and presynaptic Bassoon puncta ($p=0.18$) is unaffected in KO. (K) The number of extra-nuclear CtBP1 puncta is greatly reduced ($p=0.003$) in KO mice. (WT in blue, n = 9 mice, n puncta — CtBP1 = 19,929, Homer 4940; KO in red, n = 7 mice, n puncta — CtBP1 = 11,960, Homer = 5033). (L) Remaining CtBP1 puncta show significantly reduced ($p \leq 0.001$) pairing with postsynaptic Homer staining. Scale bars: A–D, H: 5 μm; E, F: 100 nm. Boxes represent standard deviations of the mean. Significance levels of two-tailed unpaired t-tests: n.s., not significant; *$p \leq 0.05$; **$p \leq 0.01$; ***$p \leq 0.001$.
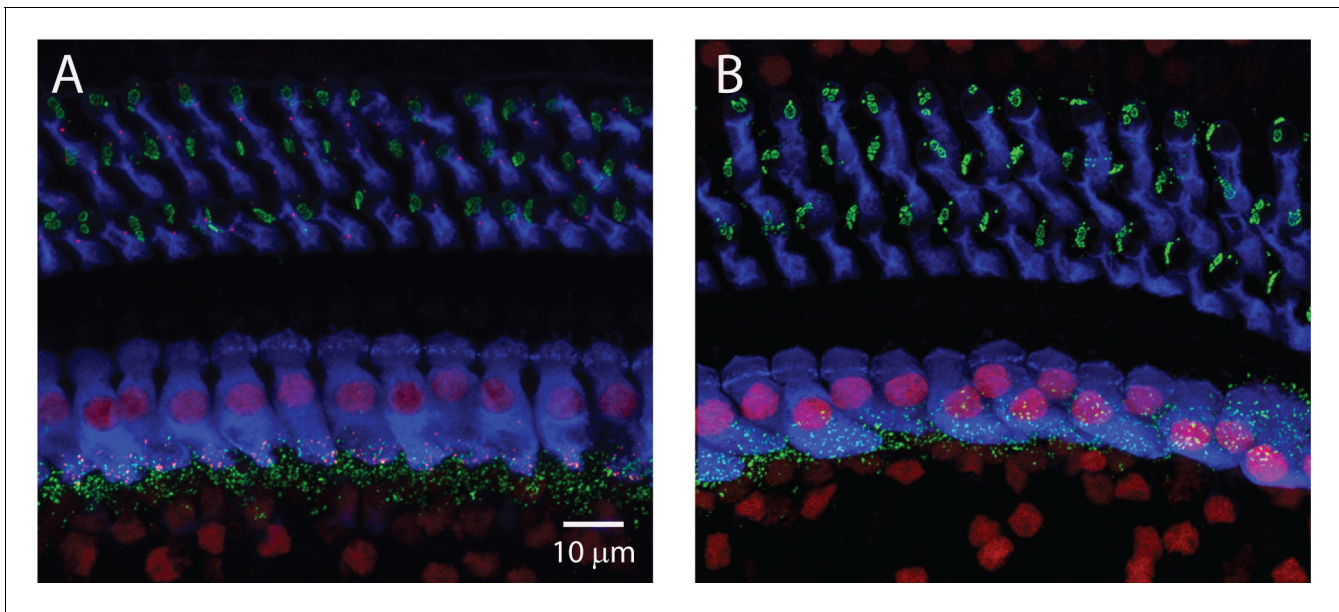
**Figure 1—figure supplement 1.** Immunohisotchemistry from WT (**A**) and KO (**B**) for Bassoon (green), CTBP2 (red) and myosin VIIa (Blue). Low-power images show that Bassoon is present in efferents of outer hair cells as well as presynaptically in IHCs. Bassoon localization is much broader than RIBEYE's and is minimally effected in the mutant animal.

DOI: https://doi.org/10.7554/eLife.30241.003
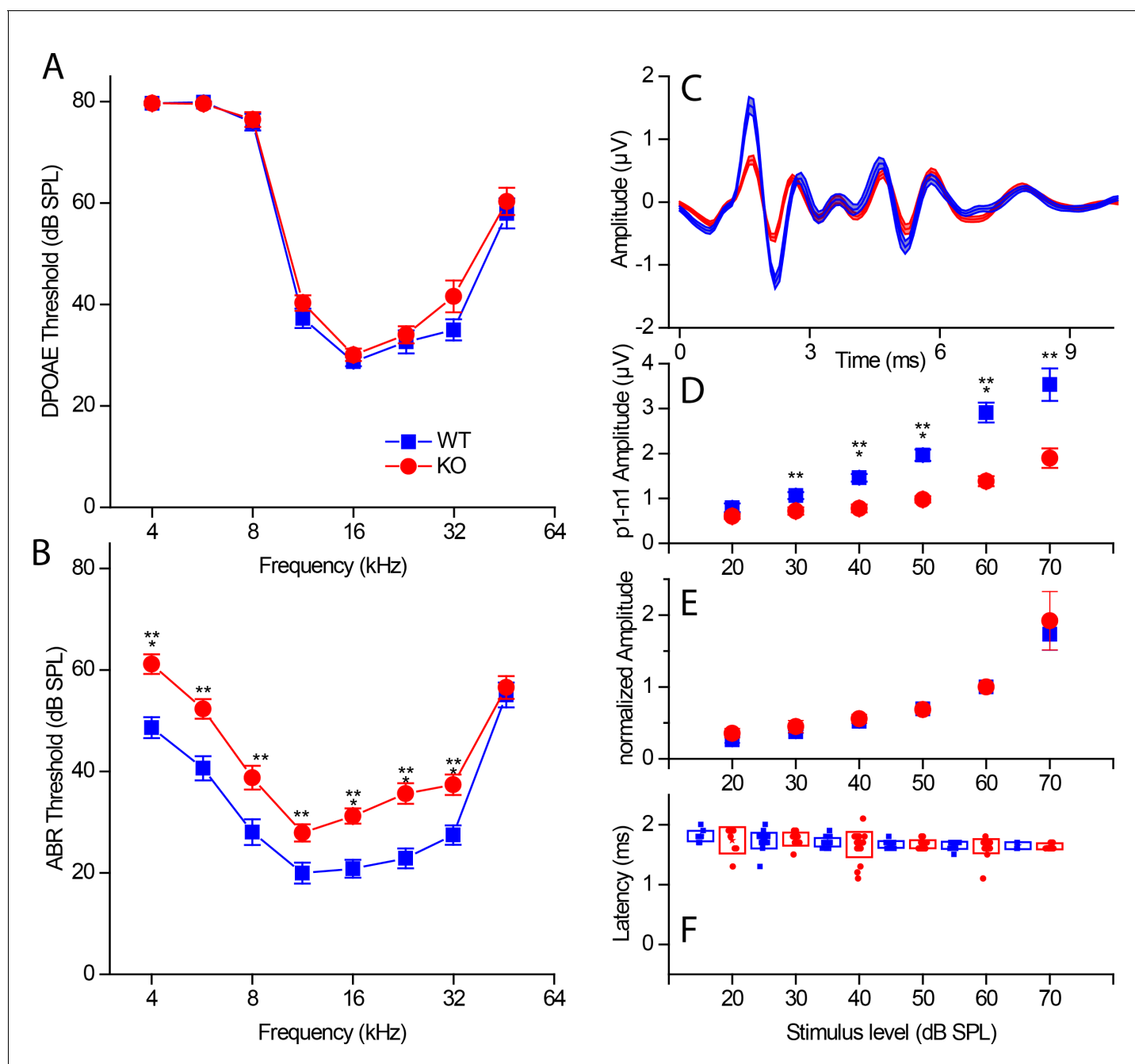
Figure 2. Hearing in RIBEYE knockout mice. (**A**) Distortion products of otoacoustic emissions (DPOAE) show no significant differences in the tested frequency range (4–46 kHz in half-octave increments) between KO (red, n = 30) and WT littermates (blue, n = 22), suggesting normal outer hair cell function. (**B**) Auditory brainstem response (ABR) measurements in the tested frequency range (4–46 kHz in half-octave increments) reveal a small (≈ 10 dB SPL) but significant threshold shift in KO mice (red, n = 28) over their WT littermates (blue, n = 22) at P21-P22. (**C**) Mean ABR waveforms to 5 ms tone pips at 23 kHz at 60 dB SPL from KO (red, n = 30) and WT littermates (blue, n = 24) reveal a decrease in amplitude of the first ABR wave in KO. (**D**) Quantification of peak to peak amplitude (wave I: p1–n1) differences between KO (red) and WT littermates (blue) at 23 kHz were significant over most sound pressure levels (20 dB SPL, p>0.05; 30 and 60 dB SPL, p≤0.01; 40–60 dB SPL, p≤0.001). (**E**) First peak amplitudes normalized to their respective values at 60 dB SPL. Amplitudes scale with their maximum value in WT and KO. (**F**) First peak latency (p1) is not significantly altered in KO mice. For wave I amplitude and latency analysis (**D–F**), the n-number varied between sound pressure levels by a clearly detectable first wave and speaker calibration, n of WT/KO — 20 dB, 11/7; 30 dB, 21/11; 40 dB, 23/22; 50 dB, 23/26; 60 dB, 23/28; 70 dB, 5/6. Boxes represent standard deviations of the mean; whiskers and the shaded line in (**C**) represent standard errors of the mean. Significance levels of two-tailed unpaired t-tests: n.s., not significant; *p≤0.05; **p≤0.01; ***p≤0.001.

DOI: https://doi.org/10.7554/eLife.30241.004
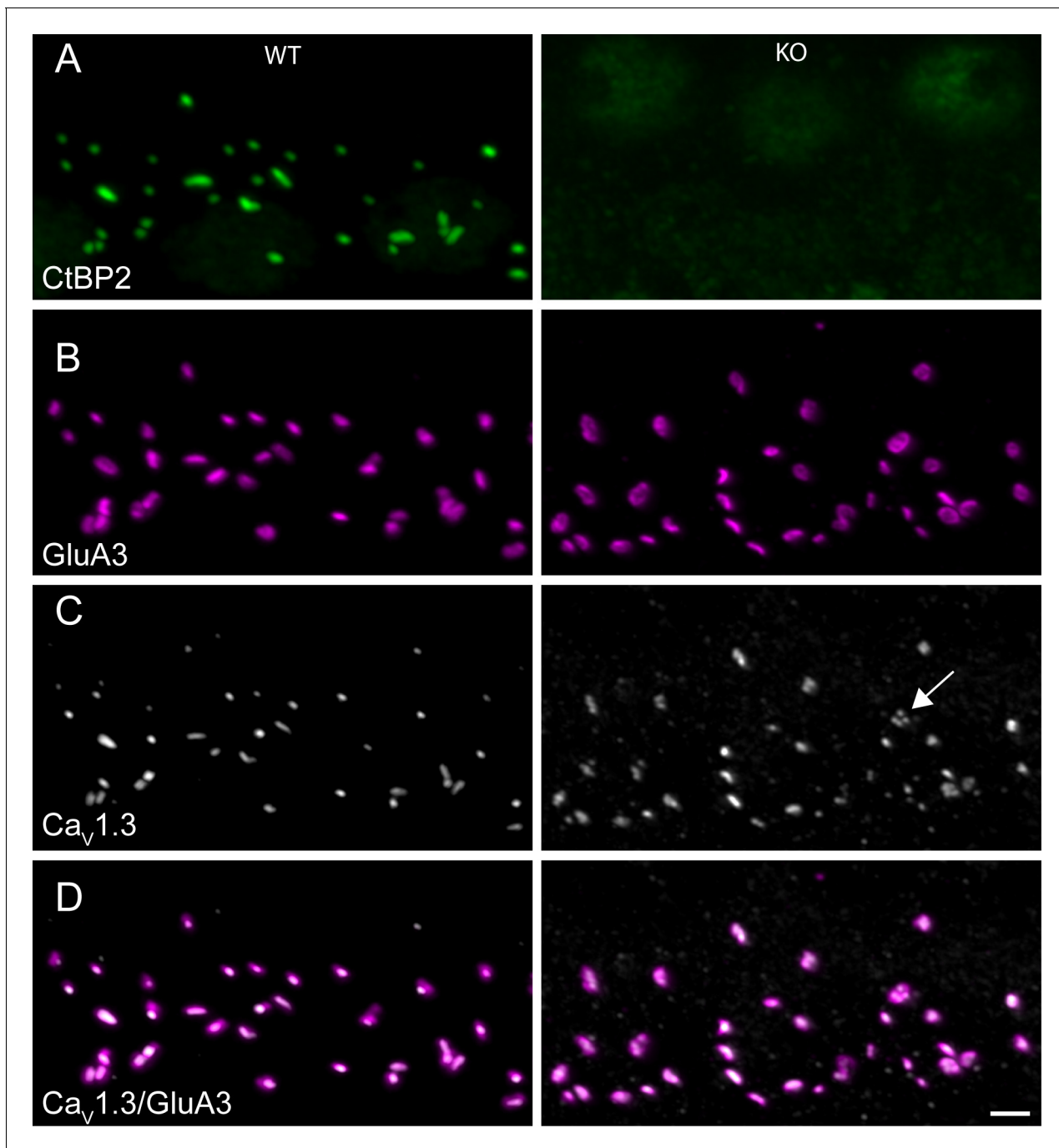
Figure 3. Ribbonless synapses contain clusters of presynaptic voltage-gated Ca^{2+} channels juxtaposed to postsynaptic glutamate receptors. (A–D) Maximum intensity projections of airyscan z-sections of IHCs in apical cochlea turns of P35 KO and WT littermates, immunolabeled for CtBP2/RIBEYE (A), GluA3 (B), Ca$_V$1.3 (C) and overlay between calcium channels and glutamate receptors (D). IHC afferent synapses from WT have a synaptic ribbon: a cytoplasmic presynaptic density comprised mainly of RIBEYE protein, recognized by anti-CtBP2 (green). The closely associated presynaptic voltage-gated Ca^{2+} channels (Ca$_V$1.3, gray) and postsynaptic AMPA receptors (GluA3, magenta) are co-labelled. IHC afferent synapses from KO lacked synaptic ribbons. The AMPA receptors in KO mice exhibited a ring-like morphology, and the Ca$_V$1.3 channels clustered in the form of round spots or elongated stripes, both similar to morphological features of WT synapses. Scale bar: 2 µm.
DOI: https://doi.org/10.7554/eLife.30241.005
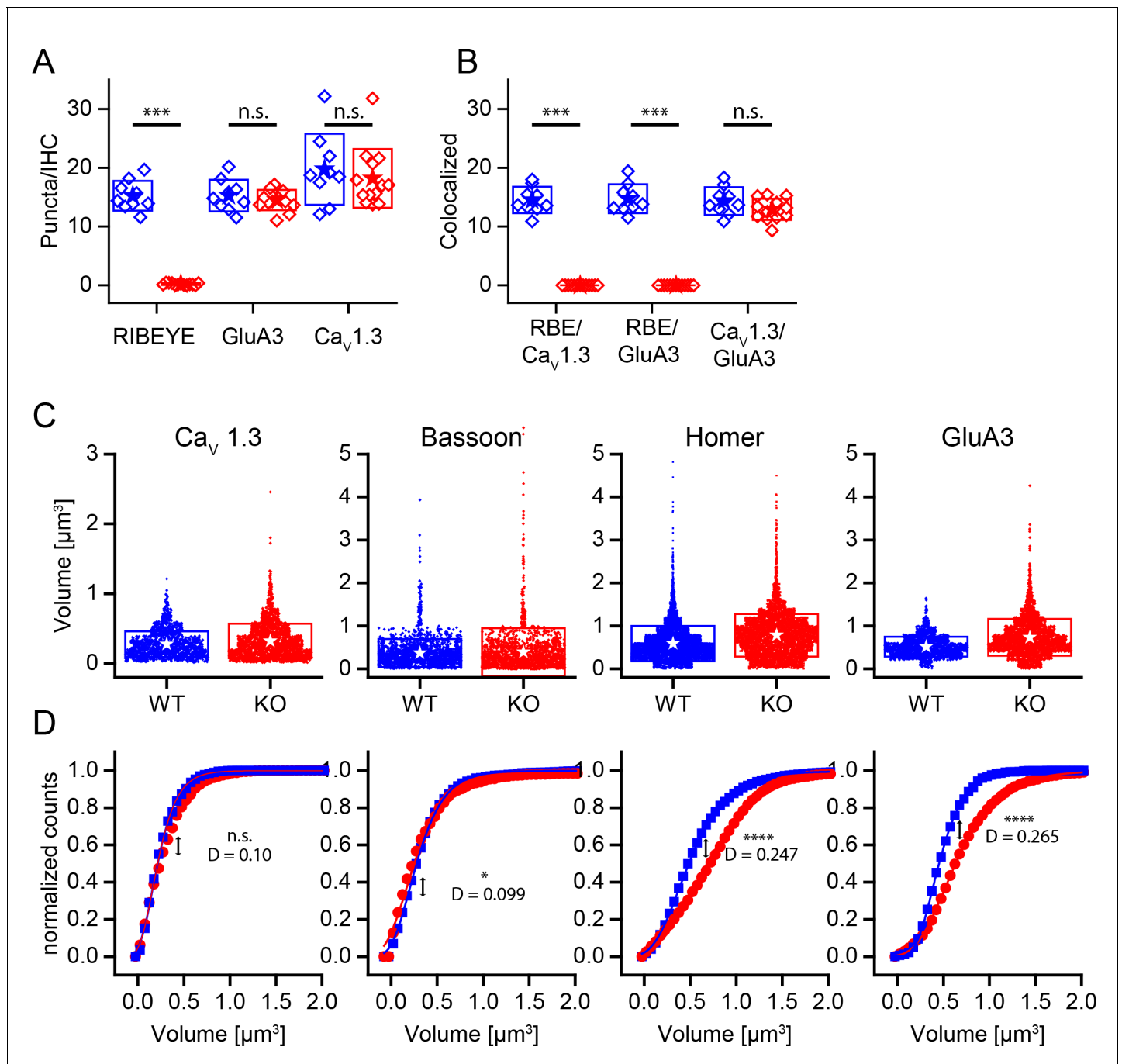
Figure 4. Changed size distribution but unaffected synapse number and organization in ribbonless synapses. (A) Quantification of RIBEYE, GluA3 and $Ca_V1.3$ puncta in the organ of corti normalized to the number of IHCs in analyzed regions of interest. The number of GluA3 receptor and $Ca_V1.3$ puncta is unaffected ($p > 0.05$). WT in blue, n = 9 images from three mice, 95 cells, quantified puncta — RIBEYE = 1456, GluA3 = 1459, $Ca_V1.3$ = 1897. KO in red, n = 13 images from three mice, 248 cells, quantified puncta — RIBEYE = 28, GluA3 = 2149, $Ca_V1.3$ = 2681. (B) Colocalization of synaptic puncta per IHC. In the absence of RIBEYE, the number of synapses, defined by colocalization of postsynaptic GluA3 and presynaptic $Ca_V1.3$, is unaffected ($p = 0.13$) in KO. (C) Volume of presynaptic $Ca_V1.3$, Bassoon and postsynaptic Homer and GluA3 in WT (blue, n synapses — $Ca_V1.3$ = 1370; Bassoon = 1917; Homer = 5219; GluA3 = 1611) and KO (red, n synapses — $Ca_V1.3$ = 2132; Bassoon = 1817; Homer = 4990; GluA3 = 2334) mice. (D) Normalized cumulative distributions of volumes show increased sizes of postsynaptic GluA3 and Homer immunoreactivity. (C) Boxes represent standard deviations of the mean. Significance levels of two-tailed unpaired t-tests (A, B) or two sample Kolmogorov-Smirnov test (C): (D) represents the maximum distance of the Kolmogorov-Smirnov distribution functions. n.s., not significant; $*p \leq 0.05$; $**p \leq 0.01$; $***p \leq 0.001$; $****p \leq 0.0001$.
DOI: https://doi.org/10.7554/eLife.30241.006
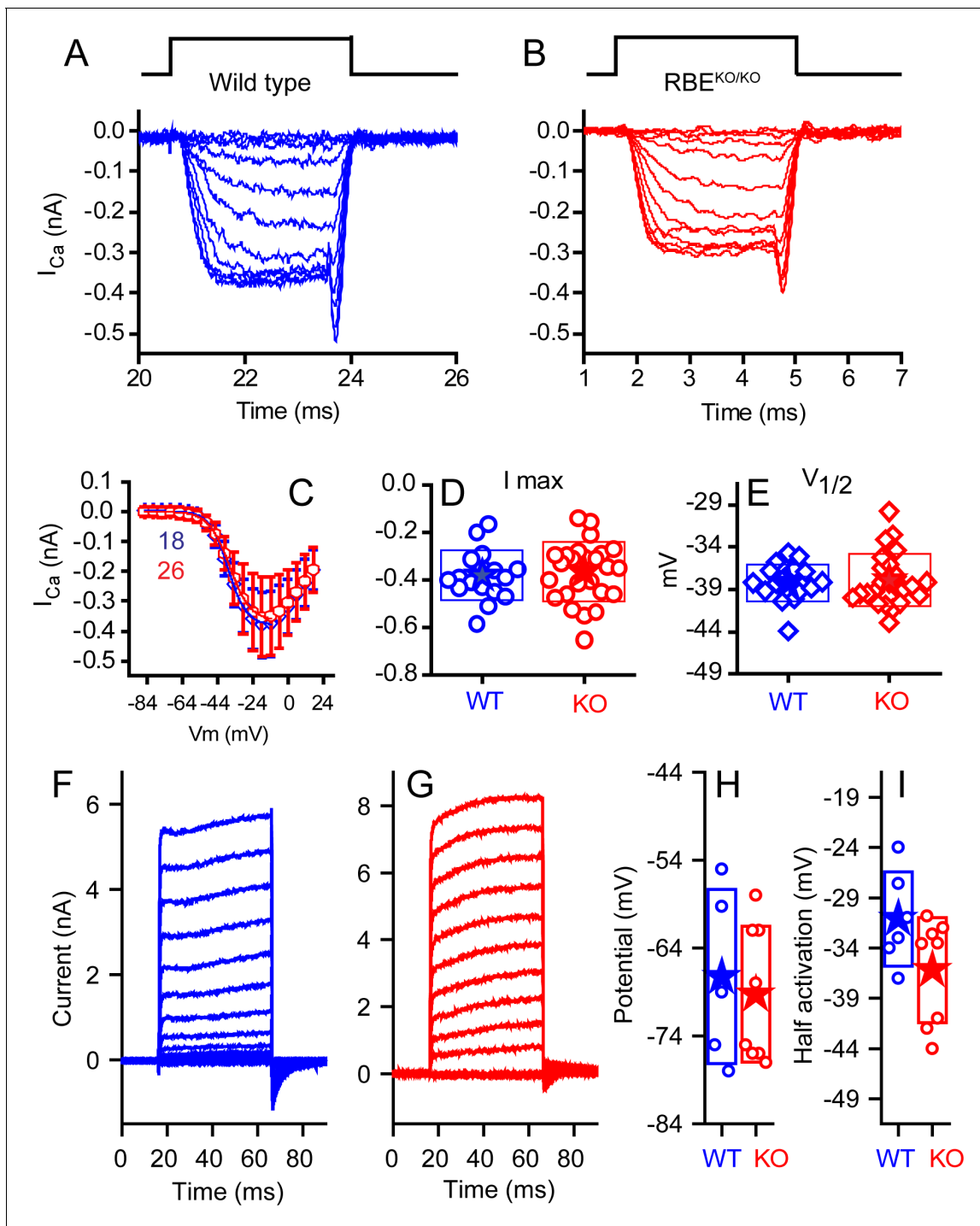
Figure 5. No differences were observed in calcium or potassium currents between KO and WT animals. Ca^{2+} currents obtained from mice ranging in age from P10–P12 for WT (A, blue) and P10–P13 KO (B, red), with time course of stimulus shown above, are comparable in all measured properties. Voltage-current plots, presented in (C) as mean ± SD show no difference (n provided in figure). Summaries of peak current (D) and voltage of half activation ($V_{1/2}$, E) are not statistically different (n = 18 for WT and n = 26 for KO, p=0.13 for peak current and 0.326 for $V_{1/2}$). Potassium currents, obtained from responses to 50 ms voltage pulses ranging from −124 mV to 16 mV in 10 mV increments, from a holding potential of −84 mV are presented in (F) for WT and (G) for KO mice at P24. A summary of the half activation voltage as estimated from a Boltzmann fit to the tail current voltage-current (H) found no statistical difference (n = 6 and 8 for WT and KO, respectively, with p=0.084). Current-clamp measurements found no difference in resting potential (I) (n = 5 and 8 for WT and KO, respectively, p=0.69).
DOI: https://doi.org/10.7554/eLife.30241.007
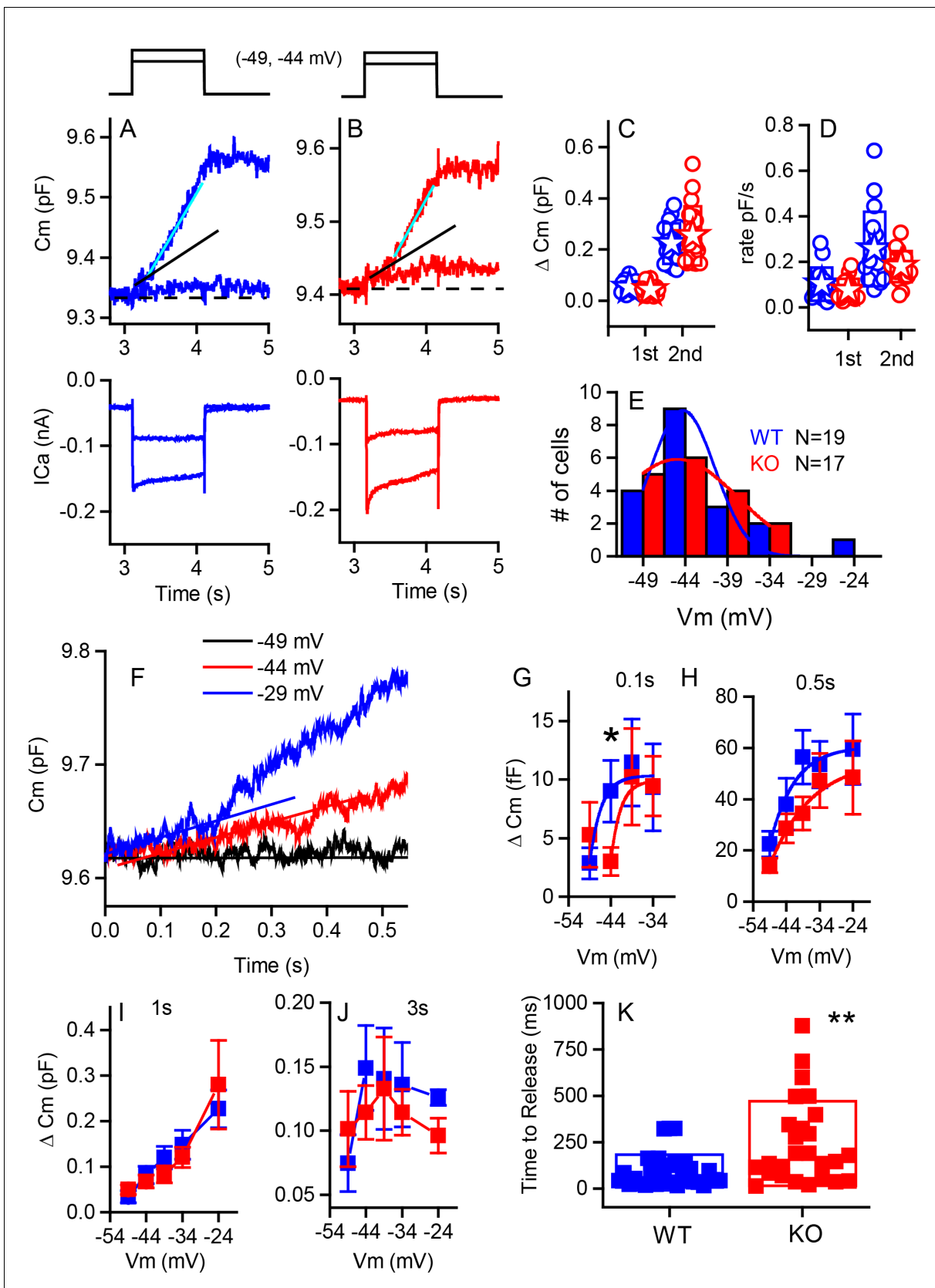
Figure 6. Capacitance responses recorded from RIBEYE knockout mice show little difference between phenotypes. Example records of Cm responses (top), showing two release components and Ca^{2+} currents (below) recorded from a WT (blue) (A) and a KO (red) mouse (B) in response to 1 s

Figure 6 continued on next page

Figure 6 continued

depolarizations from −84 mV to −49 and −44 mV. The dashed line indicates pre-stimulus baseline Cm. The black solid line indicates the first linear component of release, and the cyan line the second superlinear component. (C) Summary plot of first and second component magnitudes. No statistical difference was found between groups. For the linear component, n = 15 for WT and 15 for KO, p=0.23. For the second superlinear component, n = 17 for both groups and p=0.38. Filled stars indicate mean for this and all subsequent figures. (D) Summary plot of first and second component rates obtained by linear fits to data points, as indicated by lines in (A,B). No statistical difference was found between groups where, n = 16 for WT and 13 for KO, with p=0.266. For the second component rate, n = 17 for both groups, with p=0.085. (E) A population histogram for the voltage at which the superlinear response is first observed. Fits to Gaussian distributions show no change in the mean value but an increase in the width of the plot for the KO. (F) Example of delay in onset of capacitance change with small depolarizations for a KO cell. Plots of Cm verses voltage responses measured at 0.1 (G), 0.5 s (H) 1 s (I) or 3 s (J) show a significant difference for release at 0.1 s and −44 mV (p=0.03), error bars represent SEM. Fitting the relationships with simple exponential functions reveals differences in the shapes of the curves but not in maximum release for the 0.1 and 0.5 plots, whereas there are no differences in curve shapes for the 1 and 3 s time points. N provided in figure for each group. (K) Shows that time to release is significantly longer for KO compared to WT for depolarizations eliciting less than 50% of the maximal calcium current; n = 32 for WT and 26 for KO, p=0.0012.

DOI: https://doi.org/10.7554/eLife.30241.008
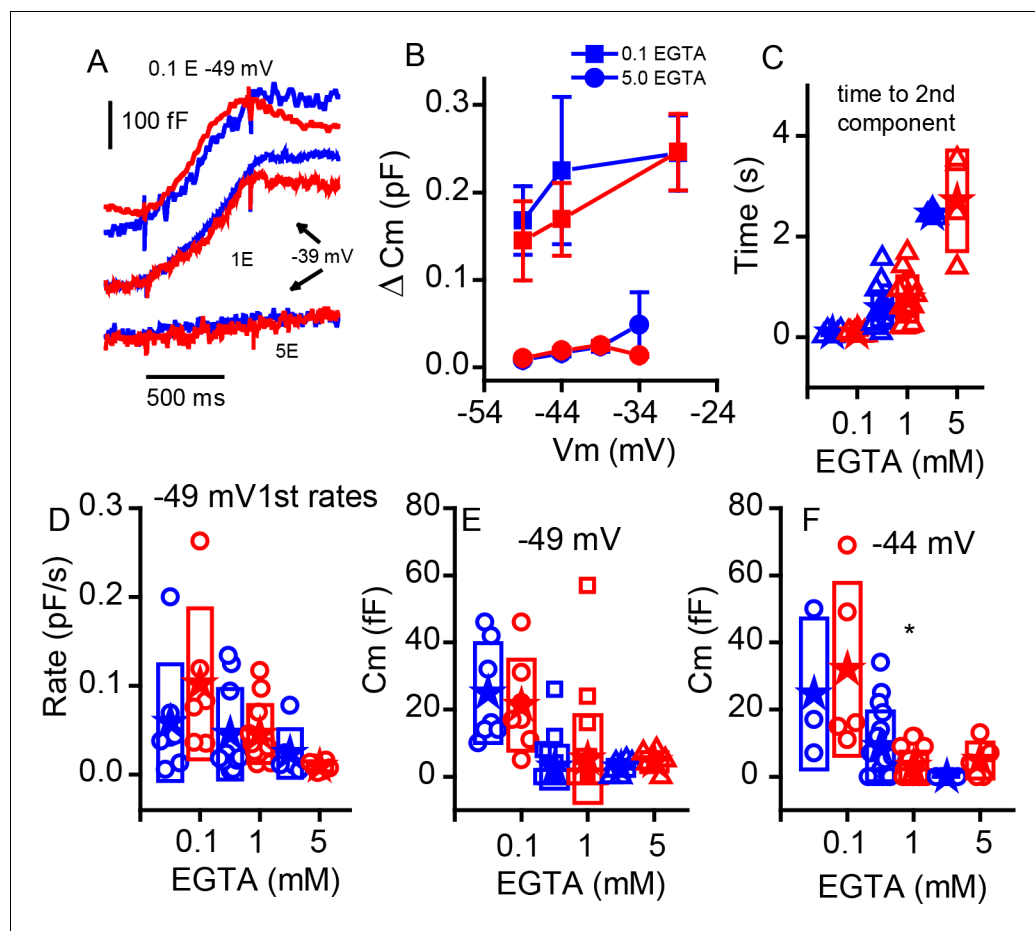
Figure 7. Changing internal Ca^{2+} buffering does not distinguish phenotypes. (A) Example records of C$_m$ changes in response to 1 s depolarizations from -49 mV in 0.1 EGTA and -39 mV in 1 and 5 mM EGTA for WT (blue) and KO (red). (B) Plot of the change in Cm in response to 1 s voltage steps of -49, -44 and -29 mV for 0.1 mM EGTA and -49, -44, -39 and -34 mV for 5 mM EGTA, n provided in figure. (C) The time to the second component increases significantly with elevated Ca^{2+} buffer (p-value indicated in figure) but is similar between genotypes: for 0.1 mM EGTA, n = 7 for WT and n = 6 for KO, p=0.93, steps to -29 mV for WT and KO; for 1 mM EGTA, n = 15 for WT and n = 13 for KO, with p=-0.13, steps to -36 ± 8 mV WT and -37 ± 9 mV KO; and for 5 mM EGTA, n = 3 for WT and n = 4 for KO, with p=0.67, steps to -39 ± 5 mV WT and -35 ± 2 mV KO. (D) The rate of release to the -49 mV step declines equally in each genotype with increasing EGTA concentration: for 0.1 mM EGTA, n = 7 for WT and n = 6 for KO, p=0.323; for 1 mM EGTA n = 20 for WT and n = 22 for KO, p=0.99; and for 5 mM EGTA, n = 7 for WT and n = 6 for KO, p=0.235. (E,F) Box plots of the first component of release for depolarizations to -49 mV (E) or -44 mV (F). The effects of buffers were similar between the two groups.

DOI: https://doi.org/10.7554/eLife.30241.009
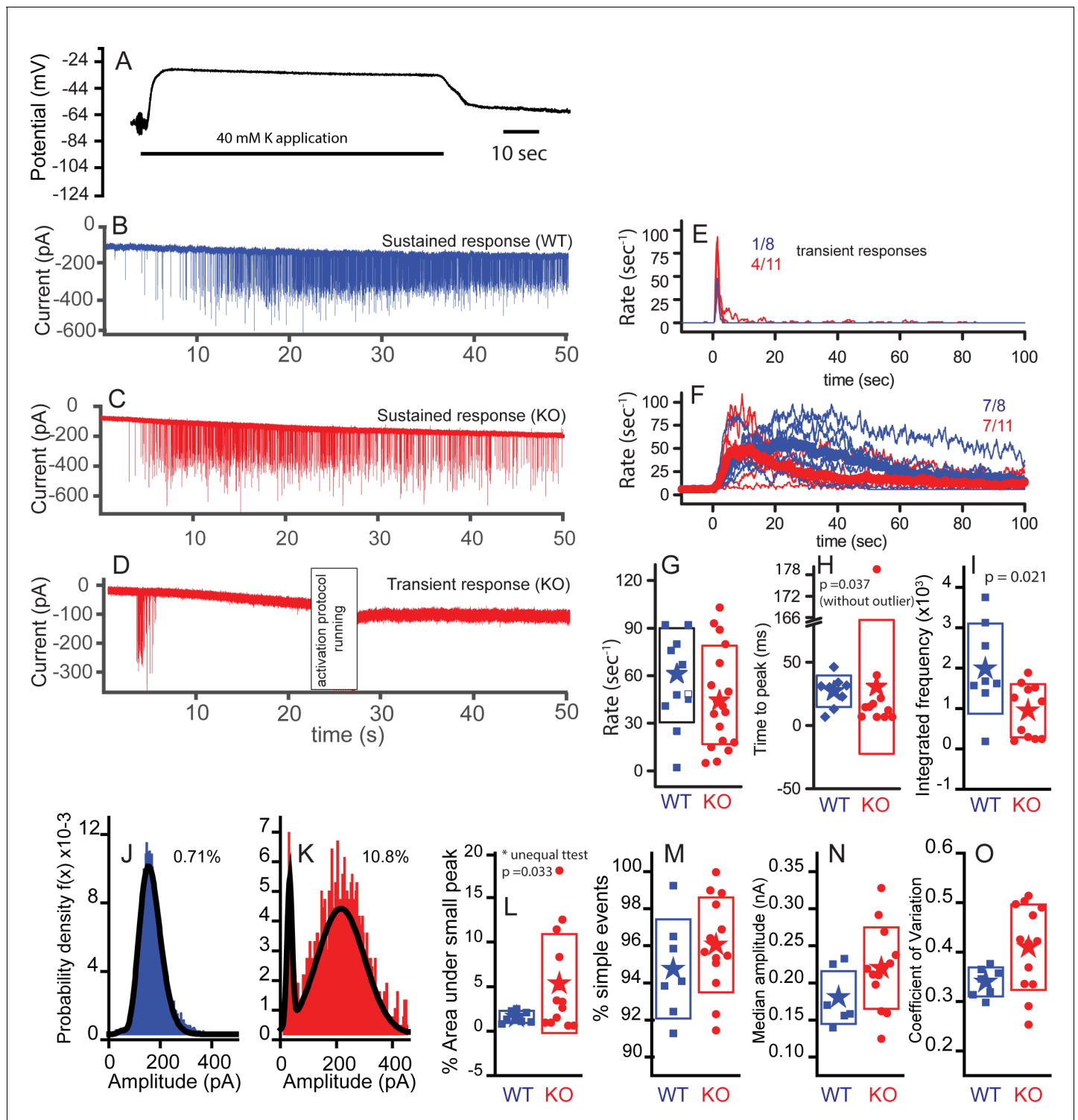
Figure 8. Subtle differences exist between WT and KO mice postsynaptic properties. Postsynaptic bouton recordings were obtained from WT or KO in control and during application of 40 mM K$^+$ to the bath. Hair cell recordings demonstrate similar depolarizations in WT and KO, suggesting that any differences in response properties may be synaptically mediated. (A) Cells rapidly recovered following washout of K$^+$. The solid line below the trace indicates the duration of the application. Postsynaptic recordings from afferent boutons in response to 40 mM K$^+$ external solution application are presented in (B) for WT and (C) for KO with a sustained response and in (D) for KO with a transient response. Recordings were made in the presence of 5 μM tetrodotoxin (TTX). Frequency responses were generated using a 1 s window sliding at 100 ms intervals (E,F). Populations were defined as transient or sustained by according to whether firing persisted after 20 s. The number of each response type is presented as a fraction in each panel.

Figure 8 continued on next page

Figure 8 continued

Maximum frequency responses are presented in box plot format with mean values shown as stars (**G**); n = 10 for WT and n = 18 for KO, p=0.313. The time to peak is presented in (**H**), where onset of K^+ application response was defined as the time point when the frequency exceeded the spontaneous frequency +3 x SD for two overlapping time windows (200 ms). The time to peak was statistically different when the one outlier was removed (time point at 181 s); n = 8 for WT and n = 10 for KO. Time to peak only includes fibers whose peak frequency reached 30 Hz, because those with lower peak frequencies had too few points to make an accurate measure. (**I**) Integrating the frequency response over 50 s shows that WT release in a more sustainable manner than the KO, n = 8 for WT and n = 10 for KO, p=0.021. Representative probability density functions for EPSC amplitudes are presented for WT (number of events = 6583) in (**J**) and for KO (number of events = 1551) in (**K**). Solid lines represent fits to either double Gaussian functions or Gaussian and gamma functions (smaller peak always fit with Gaussian function). The curves fitting the small events were integrated to measure the % of events under the small peak (shown next to each example). Only nerves that had at least 100 events are included to ensure the robustness of the fitting. (**L**) A box plot of the WT and KO percent of area contributed by the small peak. Comparisons using a t-test for unequal variance (Welch test) suggest a significant difference, p=0.032, n = 7 for WT and n = 13 for KO. (**M**) A box plot comparing the percentages of simple events, defined as single rise and decay times that are not significantly different, n = 7 for WT and n = 13 for KO, p=0.3. (**N**) Box plots of the median amplitude, where no significant difference was observed, n = 7 for WT and n = 13 for KO for each, p=0.105. (**O**) Box plots of the coefficient of variation for the distributions in (**N**). Plots were different, p=0.017, when equal variance was not assumed.

DOI: https://doi.org/10.7554/eLife.30241.010
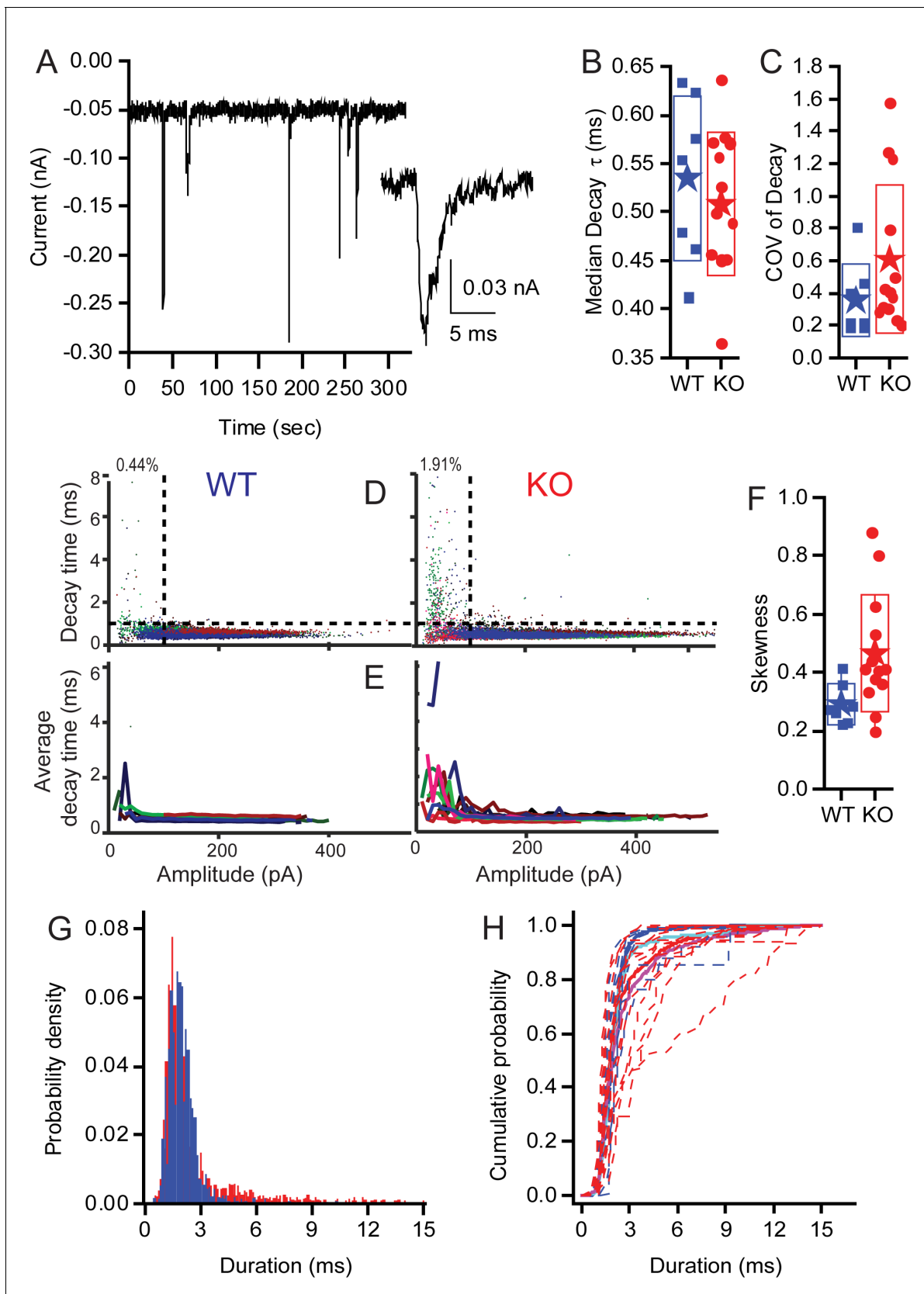
Figure 9. KO synapses have a larger population of small slow EPSCs. Seven WT fibres including 15,564 events and 13 KO fibers including 17,210 events were analyzed. (**A**) Examples of EPSCs that range in amplitude and kinetics. The inset highlights one of the small slower EPSCs identified in KO

Figure 9 continued on next page

Figure 9 continued

fibers. Median decay times (**B**) and the Coefficients of Variation for the distribution in decay times (**C**) are presented as box plots. Neither population show a statistically significant difference between the WT and KO groups. (**D**) Plots showing the skewness of the distributions of decay times and demonstrating that the KO decay time is significantly greater (away from 0), suggesting that the mean is larger than median, largely because they have a long tail of large decay time. (**E**) Plot of the EPSC decay time constant for every fiber (each fiber a different color) for both WT and KO. (**F**) Summary of the data from (**C**) as average decay time constant with EPSCs binned over 10 pA. (**G**) Pooling fibers for WT and KO recordings allowed for the generation of a probability density function for event duration. These distributions are significantly different as shown by KS test ($p < 10^{-18}$). (**H**) The cumulative probability function for the duration of EPSCs. Dashed lines are the individual fiber distributions. Solid red and blue lines represent the population aggregate (summed responses) for KO and WT, respectively. The cyan and magenta lines are the averages for WT and KO, respectively.